


 Mass Spectrometry
How to cite: *Angew. Chem. Int. Ed.* **2022**, *61*, e202200721

International Edition: doi.org/10.1002/anie.202200721

German Edition: doi.org/10.1002/ange.202200721


 Proteoform-Selective Imaging of Tissues Using Mass Spectrometry**

Manxi Yang, Hang Hu, Pei Su, Paul M. Thomas, Jeannie M. Camarillo, Joseph B. Greer, Bryan P. Early, Ryan T. Fellers, Neil L. Kelleher,* and Julia Laskin*

Abstract: Unraveling the complexity of biological systems relies on the development of new approaches for spatially resolved proteoform-specific analysis of the proteome. Herein, we employ nanospray desorption electrospray ionization mass spectrometry imaging (nano-DESI MSI) for the proteoform-selective imaging of biological tissues. Nano-DESI generates multiply charged protein ions, which is advantageous for their structural characterization using tandem mass spectrometry (MS/MS) directly on the tissue. Proof-of-concept experiments demonstrate that nano-DESI MSI combined with on-tissue top-down proteomics is ideally suited for the proteoform-selective imaging of tissue sections. Using rat brain tissue as a model system, we provide the first evidence of differential proteoform expression in different regions of the brain.

A proteome is a collection of proteins expressed by an organism, which determines its biological state. Post-translational modifications (PTM) of proteins is a process that dramatically increases the complexity of the proteome beyond what can be predicted based on the known protein-coding genes.^[1,2] PTMs affect protein structure, interactions, transport, and function thereby exhibiting a pronounced effect on cell physiology.^[3] Furthermore, the reversible nature of PTMs facilitates the dynamic response of biological systems to different conditions in both health and disease. Therefore, the identification, quantification, and

spatial mapping of proteoforms are critical to understanding biological processes.

Mass-spectrometry-based top-down proteomics is a powerful tool for proteoform characterization.^[4] This approach enables the identification of intact proteoforms based on their mass-to-charge ratio (m/z) and fragmentation pattern.^[5] Top-down proteomics has been used for the identification of thousands of proteoforms in biological samples.^[6–13] Several databases have been developed as a community resource for proteoform identification.^[14–16] Several studies used top-down proteomics for the discovery of disease biomarkers.^[17] For example, differences in the expression levels of several KRAS proteoforms have been associated with cancer cell proliferation.^[18] In another study, the phosphorylated cardiac troponin I was identified as a potential biomarker of chronic heart failure.^[19]

Although top-down proteomics is an established field, mapping of the proteoform localization in tissues is still challenging. Mass spectrometry imaging (MSI) is a label-free approach for the untargeted analysis of biomolecules with little sample preparation, which is ideally suited for spatial proteomics studies. MSI may be used for determining the spatial localization of multiple proteoforms in a single experiment, making it a powerful discovery tool for biological research.

Matrix-assisted laser desorption ionization (MALDI) has been used for imaging of intact proteins smaller than 22 kDa.^[20,21] Although a majority of these studies were performed with a moderate spatial resolution of 50 μm , a subcellular spatial resolution has been achieved using transmission-geometry MALDI source.^[22] Despite these developments, the low charge states of ions generated in MALDI presents a challenge to the detection of proteins using commercial mass spectrometers and their identification using top-down tandem mass spectrometry (MS/MS).^[23] The latter limitation has been addressed by combining MALDI MSI with the off-line protein identification using conventional top-down approaches.^[24,25] Alternatively, on-tissue protein digestion combined with bottom-up proteomics has been used for protein imaging.^[26] Nanodroplet processing in one pot for trace samples (nanoPOTs)^[27] is an emerging bottom-up technique that does not require on-tissue digestion. NanoPOTs using laser capture microdissection (LCM) enables imaging and identification of proteins in tissue sections with a spatial resolution of 50–100 μm .^[28]

Ambient ionization techniques based on liquid extraction generate higher charge states of protein ions making them suitable for conducting top-down proteomics for proteoform mapping directly from a tissue sample. Desorp-

[*] M. Yang, H. Hu, P. Su, Dr. J. Laskin
 Department of Chemistry, Purdue University
 560 Oval Drive, West Lafayette, IN 47907 (USA)
 E-mail: jlaskin@purdue.edu

P. Su, P. M. Thomas, J. M. Camarillo, J. B. Greer, B. P. Early,
 R. T. Fellers, Dr. N. L. Kelleher
 Departments of Chemistry and Molecular Biosciences,
 Northwestern University
 2145 Sheridan Road, Evanston, IL 60208 (USA)
 E-mail: n-kelleher@northwestern.edu

[**] A previous version of this manuscript has been deposited on a preprint server (<https://doi.org/10.33774/chemrxiv-2021-wtjm2>).

© 2022 The Authors. Angewandte Chemie International Edition published by Wiley-VCH GmbH. This is an open access article under the terms of the Creative Commons Attribution Non-Commercial License, which permits use, distribution and reproduction in any medium, provided the original work is properly cited and is not used for commercial purposes.

tion electrospray ionization (DESI) and liquid extraction surface analysis (LESA) have been used for detecting intact proteins in tissues.^[29] DESI has been used for imaging of <20 kDa proteins with a spatial resolution of 150–200 μm .^[30,31] Meanwhile, the localization of larger proteins and protein complexes of up to 47 kDa has been examined using LESA with a spatial resolution of 600 μm .^[32,33]

Nanospray desorption electrospray ionization (nano-DESI) is an ambient ionization technique, which has been extensively used for imaging of lipids and metabolites with high sensitivity and a spatial resolution down to 10 μm .^[34] Although the utility of nano-DESI for protein analysis has been demonstrated,^[35] only a few studies used it for protein imaging. In particular, nano-DESI MSI has been used for protein localization in healthy and MYC-induced lymphoma mouse brain tissue sections,^[36] imaging of proteins in skin melanoma,^[37] and native MSI of protein complexes in rat kidney tissues.^[38,39]

Despite the impressive developments in spatial proteomics, the direct imaging and identification of proteoforms has not advanced significantly in recent years. In this study, we utilize nano-DESI MSI combined with top-down proteomics directly on a tissue for imaging of proteoforms. Proof-of-concept experiments presented herein used rat brain tissue sections to demonstrate the ability of nano-DESI MSI to generate high-quality proteoform-specific imaging data. Proteoforms with unique PTMs were selected to generate ion images. We observed forty proteoforms of nineteen <19 kDa proteins, among which we identified fifteen proteoforms with confidence level 1, nine proteoforms with confidence level 2A, one proteoform with confidence level 3, and ten proteoforms with confidence level 4.^[40] We also investigated the relative abundance of multiple proteoforms of the 14.1 kDa myelin basic protein (MBP) across the tissue. Our results provide first insights into the differences in proteoform expression levels in different regions of the brain, which is important for understanding the relevant biological pathways.

Nano-DESI MSI and on-tissue top-down proteomics experiments are described in detail in the Supporting Information. Briefly, rat brain tissue sections were delipidated by sequential washes in ethanol solutions (70 %, 90 %, and 100 %) and chloroform right before the analysis. Proteoforms were extracted into the liquid bridge formed between two fused capillaries and ionized by electrospray ionization at a mass spectrometer inlet. ACN/H₂O/CH₃COOH (65/34/1, v/v/v) was used as the extraction solvent. On-tissue top-down proteomics analysis was performed using targeted MS/MS. Proteoforms were identified by matching their intact masses and MS/MS data against the *Rattus norvegicus* (Rat: Taxon 10116) database.

Representative mass spectra from two regions of the brain tissue are shown in Figure 1. The 14.1 kDa MBP is the most abundant species detected in the white matter region of the cerebellum (Figure 1a). We observe the unmodified 14.1 kDa MBP and 10 PTMs with the charge state distribution in the range of +15 to +26. The most abundant proteoforms and their intact masses are listed in Figure 1c. We also detected an 18.4 kDa isoform of MBP and its two

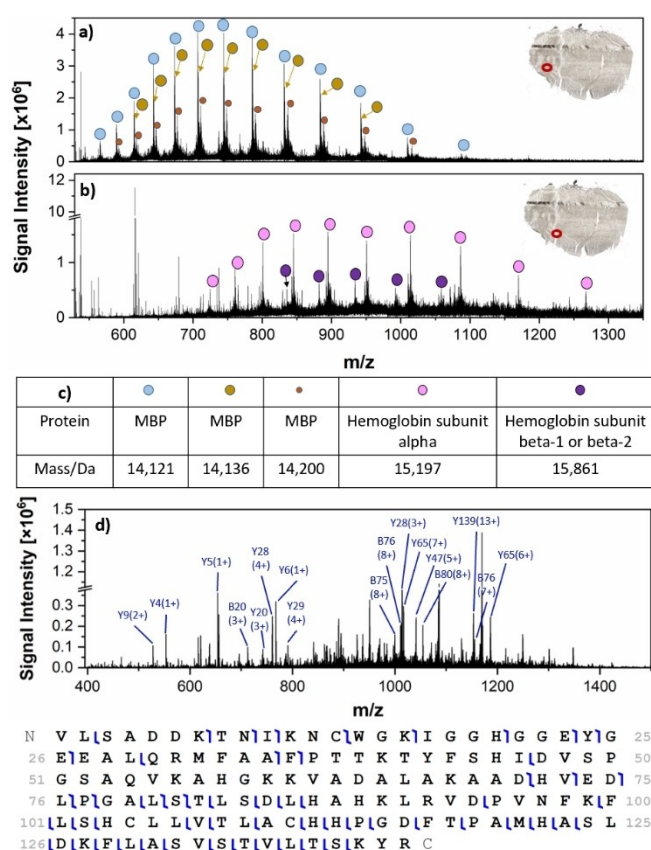


Figure 1. Average mass spectra of the rat brain tissue showing protein signals in the a) white matter and b) blood vessel regions highlighted with red circles in the corresponding optical images. c) A table summarizing the features labeled in (a) and (b). d) MS/MS spectrum of the unmodified hemoglobin subunit alpha (HBA1) and its fragmentation map obtained using the normalized collision energy (NCE) of 23 and isolation window of 3 m/z .

PTMs in the white matter region. In addition to MBPs, we observe abundant signals of hemoglobin proteoforms in the blood vessel region (Figure 1b). The mass spectrum obtained for this region contains the charge state distribution of hemoglobin subunit alpha (HBA1), subunit beta-1 (HBB1), and beta-2 (HBB2) with a total of 13 proteoforms in the range of +11 to +20. The top two most abundant proteoforms are listed in Figure 1c. Figure 1d shows the annotated MS/MS spectrum of the unmodified HBA1 and its corresponding fragmentation map with 41 % sequence coverage. Most of the other proteoforms detected in this study are enhanced in the hippocampal formation region. A representative averaged mass spectrum obtained from this region is shown in Figure S2. A complete list of the proteoforms identified and imaged in this study with their proteoform identification levels is provided in the supporting table.^[40] Top-down MS/MS data for all the proteoforms with levels 1, 2A and 3 identifications are shown in Figures S13–S36. MS/MS spectra for proteoforms with level 4 identification are shown in Figures S37–S46.

Ion images of several abundant proteoforms normalized to the total ion current (TIC) are shown in Figure 2. An

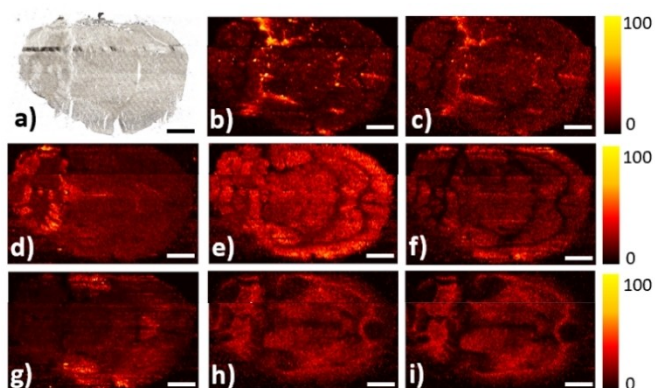


Figure 2. a) An optical image of an axial rat brain tissue section after nano-DESI MSI analysis. Ion images of the intact proteins normalized to TIC: b) m/z 894.9384¹⁷⁺, 15 197 Da, hemoglobin subunit alpha (HBA1), unmodified (level 1), c) m/z 992.281¹⁶⁺, 15 861 Da, hemoglobin subunit beta-1 (HBB-1), R104 di-methylation (level 1), d) m/z 765.4067¹³⁺, 9937 Da, acyl-CoA-binding protein (ACBP), acetylation (level 2A), e) m/z 784.564⁷⁺, 5 485 Da, cytochrome c oxidase subunit 7c, mitochondrial (COX7c), unmodified (level 1), f) m/z 998.7947¹⁰⁺, 9978 Da, cytochrome c oxidase subunit 6B1 (COX6B1), N-terminal acetylation (level 1), g) m/z 709.9375⁷⁺, 4 963 Da, thymosin beta-4, acetylation (level 2A), h) m/z 741.8094¹⁹⁺, 14 075 Da, myelin basic protein (MBP), unmodified (level 1), i) m/z 682.3572²⁷⁺, 18 397 Da, myelin basic protein (MBP), N-terminal acetylation (level 1). Scale bar: 3 mm.

optical image of the analyzed section is shown in Figure 2a. Additional images are provided in Figure S3. Ion images of the same proteoforms obtained in replicate experiments are shown in Figures S4 and S5. The two most abundant proteoforms of hemoglobin, unmodified HBA1 (Figure 2b) and di-methylated HBB-1 (Figure 2c) are enhanced in the blood vessel region. Similar localization is observed for all the hemoglobin proteoforms. The observed localization of hemoglobin proteoforms to the blood vessel region validates the proteoform-selective imaging experiments. Additional ion images of hemoglobin in replicate experiments are shown in Figures S10, S11, and S12.

Figure 2d shows the unique distribution of the acetylated acyl-CoA binding protein (ACBP) enhanced in the grey matter region of the rat brain cerebellum. ACBP functions as a transporter of both medium- and long-chain acyl-CoA esters. The observed enhancement of the ACBP in the grey matter is consistent with its previously reported localization to the glial cells and synaptosomal nerve ending, the major components of the grey matter in rat brain.^[41] Both the unmodified mitochondrial cytochrome c oxidase, subunit 7c (Figure 2e) and N-terminal acetylated cytochrome c oxidase 6B1 (Figure 2f) are evenly distributed across the rat brain tissue. Figure 2g displays the localization of the acetylated 4.9 kDa thymosin beta-4, which is enhanced in the hippocampal formation, isocortex, lateral septal nucleus, and ventral striatum regions. This distribution is consistent with the high expression level of thymosin beta-4 messenger RNA (mRNA) in the hippocampal formation and cerebral cortex regions.^[42,43] A similar localization is observed for the acetylated 4.7 kDa isoform of thymosin beta-4 (Figure S4t).

Ion images of the two isoforms of MBP, unmodified 14.1 kDa MBP and N-terminal acetylated 18.4 kDa MBP (Figure 2h,i), indicate a similar localization of these two proteins in rat brain tissue. The signals of MBPs are enhanced in midbrain and white matter regions of the brain. MBPs are abundant proteins in the myelin sheath essential for the formation of myelin and associated with protein transport and signaling.^[44,45]

MBP and hemoglobin are the two proteins with most PTMs detected in this study. A region of the mass spectrum containing the +19 charge state of 14.1 kDa MBP proteoforms and +25 charge state of 18.4 kDa MBP proteoforms is shown in Figure S6. Figure 3 shows ion images of six MBP proteoforms. Ion images of all the eleven MBP proteoforms are shown in Figure S7. Additional ion images obtained in replicate experiments are shown in Figure S8 and S9 to demonstrate reproducibility. All the proteoforms have similar spatial distributions, which is consistent with the expression of their coding genes in specific regions. However, the relative abundances of different proteoforms vary across the tissue. These differences are visualized using ratio images shown under each ion image in Figure 3. The ratio images were generated by plotting the ratio of the individual proteoform signal to the sum of signals of all the MBP proteoforms in the +19 charge state in each pixel of the image. The ratio images reveal the expression of each proteoform in different regions of the brain tissue.

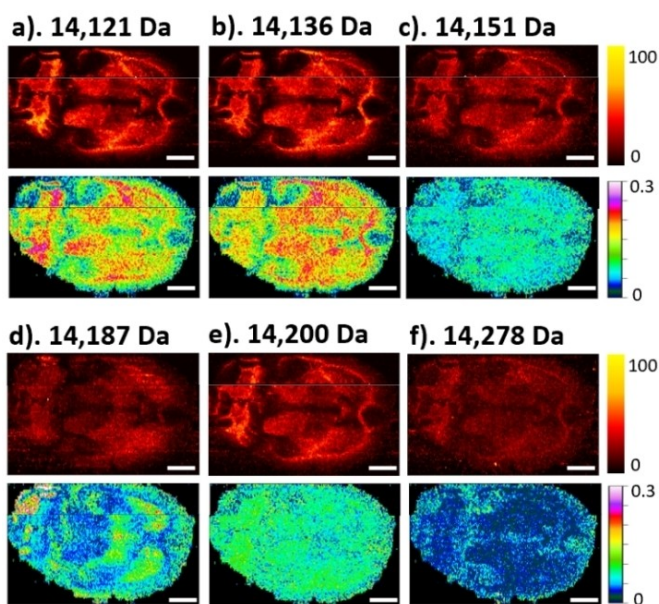


Figure 3. Ion images of the +19 charge state of the 14.1 kDa MBP proteoforms. Top panels show ion images normalized to the TIC. Bottom panels show images generated by plotting the ratio of the individual proteoform signal to the sum of signals of all the MBP proteoforms: a) m/z 744.2335¹⁹⁺, 14 121 Da, N-terminal acetylation (level 1), b) m/z 745.0235¹⁹⁺, 14 136 Da, N-terminal acetylation, methionine sulfoxide (level 1), c) m/z 745.8132¹⁹⁺, 14 151 Da, phosphorylation (level 3), d) m/z 747.7063¹⁹⁺, 14 187 Da, di-methylation, phosphorylation (level 2A), e) m/z 748.3901¹⁹⁺, 14 200 Da, N-terminal acetylation, phosphorylation (level 2A), f) m/z 752.4923¹⁹⁺, 14 278 Da, N-terminal acetylation, di-phosphorylation (level 2A). Scale bar: 3 mm.

Both the N-terminal acetylated MBP (Figure 3a) and its oxidized form (Figure 3b) are enhanced in the midbrain and white matter regions. However, the N-terminal acetylated MBP (Figure 3a) is more abundant in the white matter of the cerebellum region whereas the oxidized form is more abundant in the midbrain region (Figure 3b). Methionine oxidation is a spontaneous PTM attributed to oxidative damage, which accumulates with aging.^[46] Methionine sulfoxide reductase (MSR) repairs the oxidative damage by reducing methionine sulfoxide to methionine.^[46] This observed difference in the relative abundance of the two proteoforms may be attributed to the higher activity of MSR in the cerebellum region in comparison with other regions of the brain.^[47]

The ratio images of the phosphorylated MBP (Figure 3c) and its N-terminal acetylated form (Figure 3e) display a uniform distribution across the entire tissue section. However, the ratio image of the N-terminal acetylated, di-phosphorylated MBP (Figure 3f) shows the enhanced abundance of this proteoform in the hippocampal formation and isocortex regions. An interesting ratio image showing an enhanced abundance in the thalamus and striatum ventral region was observed for the di-methylated, phosphorylated MBP (Figure 3d).

In summary, the combination of on-tissue top-down proteomics with nano-DESI MSI has been used to generate first proteoform-selective images of a rat brain tissue. We obtained spatial maps of forty proteoforms of nineteen distinct proteins with twenty-five proteoforms identified with confidence levels 1, 2A and 3. Ratio images reveal the differential expression of the individual proteoforms in different parts of the tissue. Although this proof-of-concept study focused on proteoforms of abundant proteins, the observed differential proteoform localization in tissue sections demonstrates the power of this approach for studying the state of different cell types in biological tissues. Several strategies may be used to improve the detection of a broader range of proteoforms. These include spectral deconvolution,^[48–50] coupling of nano-DESI MSI with ion mobility separation,^[39,51] and single ion detection.^[52,53] Furthermore, sequence coverage in top-down identification experiments may be improved by improving the signals and using complementary fragmentation approaches such as electron transfer dissociation (ETD).^[54–56] Proteoform-selective imaging opens opportunities for mapping of differentially modified proteoforms to functional units within tissues. As the technology is pushed toward the single cell level, the exploration of proteoforms in specific cell types in human tissues will be possible, thus advancing our understanding of proteoform function and their exploitation as disease biomarkers.

Acknowledgements

The authors gratefully acknowledge the financial support from the National Institutes of Health (NIH) Common Fund, through the Office of Strategic Coordination/Office of the NIH Director under awards UG3HL145593 and

UH3CA255132 (HuBMAP Program, J.L.), UH3CA246635 (HuBMAP Program, N.L.K.), and P41GM108569 (N.L.K.), and the support from National Science Foundation (NSF) under awards #1916691 (Center for Bioanalytic Metrology, J.L.). MSI data analysis tools used in this study were developed with support from NSF-1808136 and NSF-2108729 (J.L.). We thank Drs. Elizabeth K. Neumann and Jeffrey M. Spraggins (Vanderbilt University) for providing rat brain tissue sections.

Conflict of Interest

The authors declare no conflict of interest.

Data Availability Statement

The data that support the findings of this study are available in the Supporting Information of this article.

Keywords: Mass Spectrometry Imaging · Post-Translational Modifications · Proteoforms · On-Tissue Top-down Proteomics

- [1] R. Aebersold, J. N. Agar, I. J. Amster, M. S. Baker, C. R. Bertozzi, E. S. Boja, C. E. Costello, B. F. Cravatt, C. Fenselau, B. A. Garcia, Y. Ge, J. Gunawardena, R. C. Hendrickson, P. J. Hergenrother, C. G. Huber, A. R. Ivanov, O. N. Jensen, M. C. Jewett, N. L. Kelleher, L. L. Kiessling, N. J. Krogan, M. R. Larsen, J. A. Loo, R. R. Ogorzalek Loo, E. Lundberg, M. J. Maccoss, P. Mallick, V. K. Mootha, M. Mrksich, T. W. Muir, S. M. Patrie, J. J. Pesavento, S. J. Pitteri, H. Rodriguez, A. Saghatelian, W. Sandoval, H. Schlüter, S. Sechi, S. A. Slavoff, L. M. Smith, M. P. Snyder, P. M. Thomas, M. Uhlén, J. E. Van Eyk, M. Vidal, D. R. Walt, F. M. White, E. R. Williams, T. Wohlschläger, V. H. Wysocki, N. A. Yates, N. L. Young, B. Zhang, *Nat. Chem. Biol.* **2018**, *14*, 206–214.
- [2] L. M. Smith, N. L. Kelleher, *Nat. Methods* **2013**, *10*, 186–187.
- [3] R. B. Parekh, C. Rohlf, *Curr. Opin. Biotechnol.* **1997**, *8*, 718–723.
- [4] F. Lermite, Y. O. Tsybin, P. B. O'Connor, J. A. Loo, *J. Am. Soc. Mass Spectrom.* **2019**, *30*, 1149–1157.
- [5] N. Siuti, N. L. Kelleher, *Nat. Methods* **2007**, *4*, 817–821.
- [6] E. N. Mccool, R. A. Lubeckyj, X. Shen, D. Chen, Q. Kou, X. Liu, L. Sun, *Anal. Chem.* **2018**, *90*, 5529–5533.
- [7] J. C. Tran, L. Zamdborg, D. R. Ahlf, J. E. Lee, A. D. Catherman, K. R. Durbin, J. D. Tipton, A. Vellaichamy, J. F. Kellie, M. Li, C. Wu, S. M. M. Sweet, B. P. Early, N. Siuti, R. D. Leduc, P. D. Compton, P. M. Thomas, N. L. Kelleher, *Nature* **2011**, *480*, 254–258.
- [8] M. Dupré, M. Dupré, M. Duchateau, C. Malosse, D. Borges-Lima, V. Calvaresi, I. Podglajen, D. Clermont, M. Rey, J. Chamot-Rooke, *J. Proteome Res.* **2021**, *20*, 202–211.
- [9] M. Zhou, N. Uwugiaren, S. M. Williams, R. J. Moore, R. Zhao, D. Goodlett, Y. Zhu, *Anal. Chem.* **2020**, *92*, 7087–7095.
- [10] D. Yu, Z. Wang, K. A. Cupp-Sutton, Y. Guo, Q. Kou, K. Smith, X. Liu, S. Wu, *J. Am. Soc. Mass Spectrom.* **2021**, *32*, 1336–1344.
- [11] M. R. Mehaffey, Q. Xia, J. S. Brodbelt, *Anal. Chem.* **2020**, *92*, 15202–15211.

- [12] L. V. Schaffer, L. C. Anderson, D. S. Butcher, M. R. Shortreed, R. M. Miller, C. Pavelec, L. M. Smith, *J. Proteome Res.* **2021**, *20*, 317–325.
- [13] N. D. Schmitt, J. M. Berger, J. B. Conway, J. N. Agar, *Anal. Chem.* **2021**, *93*, 6355–6362.
- [14] Y. Dai, K. E. Buxton, L. V. Schaffer, R. M. Miller, R. J. Millikin, M. Scalf, B. L. Frey, M. R. Shortreed, L. M. Smith, *J. Proteome Res.* **2019**, *18*, 3671–3680.
- [15] J. Park, P. D. Piehowski, C. Wilkins, M. Zhou, J. Mendoza, G. M. Fujimoto, B. C. Gibbons, J. B. Shaw, Y. Shen, A. K. Shukla, R. J. Moore, T. Liu, V. A. Petyuk, N. Tolić, L. Paša-Tolić, R. D. Smith, S. H. Payne, S. Kim, *Nat. Methods* **2017**, *14*, 909–914.
- [16] C. Lantz, M. A. Zenaidee, B. Wei, Z. Hemminger, R. R. Ogorzalek Loo, J. A. Loo, *J. Proteome Res.* **2021**, *20*, 1928–1935.
- [17] L. Smith, J. Agar, J. Chamot-Rooke, P. Danis, Y. Ge, J. Loo, L. Pasa-Tolic, Y. Tsybin, N. Kelleher, *Sci. Adv.* **2021**, *7*, eabk0734.
- [18] I. Ntai, L. Fornelli, C. J. Dehart, J. E. Hutton, P. F. Doubleday, R. D. Leduc, A. J. Van Nispen, R. T. Fellers, G. Whiteley, E. S. Boja, H. Rodriguez, N. L. Kelleher, *Proc. Natl. Acad. Sci. USA* **2018**, *115*, 4140–4145.
- [19] J. Zhang, M. J. Guy, H. S. Norman, Y.-C. Chen, Q. Xu, X. Dong, H. Guner, S. Wang, T. Kohmoto, K. H. Young, R. L. Moss, Y. Ge, *J. Proteome Res.* **2011**, *10*, 4054–4065.
- [20] B. M. Prentice, D. J. Ryan, R. Van De Plas, R. M. Caprioli, J. M. Spraggins, *Anal. Chem.* **2018**, *90*, 5090–5099.
- [21] R. M. Caprioli, *J. Biomol. Tech.* **2019**, *30*, 7–11.
- [22] A. Zavalin, J. Yang, K. Hayden, M. Vestal, R. M. Caprioli, *Anal. Bioanal. Chem.* **2015**, *407*, 2337–2342.
- [23] D. J. Ryan, J. M. Spraggins, R. M. Caprioli, *Curr. Opin. Chem. Biol.* **2019**, *48*, 64–72.
- [24] D. J. Ryan, N. H. Patterson, N. E. Putnam, A. D. Wilde, A. Weiss, W. J. Perry, J. E. Cassat, E. P. Skaar, R. M. Caprioli, J. M. Spraggins, *Anal. Chem.* **2019**, *91*, 7578–7585.
- [25] H. Ye, R. Mandal, A. Catherman, P. M. Thomas, N. L. Kelleher, C. Ikonomidou, L. Li, *PLoS One* **2014**, *9*, e92831.
- [26] B. Cillero-Pastor, R. M. A. Heeren, *J. Proteome Res.* **2014**, *13*, 325–335.
- [27] Y. Zhu, P. D. Piehowski, R. Zhao, J. Chen, Y. Shen, R. J. Moore, A. K. Shukla, V. A. Petyuk, M. Campbell-Thompson, C. E. Mathews, R. D. Smith, W.-J. Qian, R. T. Kelly, *Nat. Commun.* **2018**, *9*, 882.
- [28] P. D. Piehowski, Y. Zhu, L. M. Bramer, K. G. Stratton, R. Zhao, D. J. Orton, R. J. Moore, J. Yuan, H. D. Mitchell, Y. Gao, B. J. M. Webb-Robertson, S. K. Dey, R. T. Kelly, K. E. Burnum-Johnson, *Nat. Commun.* **2020**, *11*, 8.
- [29] R. L. Griffiths, K. I. Kocurek, H. J. Cooper, *Curr. Opin. Chem. Biol.* **2018**, *42*, 67–75.
- [30] M. W. Towers, T. Karancsi, E. A. Jones, S. D. Pringle, E. Claude, *J. Am. Soc. Mass Spectrom.* **2018**, *29*, 2456–2466.
- [31] K. Y. Garza, C. L. Feider, D. R. Klein, J. A. Rosenberg, J. S. Brodbelt, L. S. Eberlin, *Anal. Chem.* **2018**, *90*, 7785–7789.
- [32] O. J. Hale, E. K. Sisley, R. L. Griffiths, I. B. Styles, H. J. Cooper, *J. Am. Soc. Mass Spectrom.* **2020**, *31*, 873–879.
- [33] O. J. Hale, H. J. Cooper, *J. Am. Soc. Mass Spectrom.* **2020**, *31*, 2531–2537.
- [34] R. Yin, K. E. Burnum-Johnson, X. Sun, S. K. Dey, J. Laskin, *Nat. Protoc.* **2019**, *14*, 3445–3470.
- [35] P. J. Roach, J. Laskin, A. Laskin, *Analyst* **2010**, *135*, 2161–2452.
- [36] C. Hsu, P. Chou, R. N. Zare, *Anal. Chem.* **2015**, *87*, 11171–11175.
- [37] C.-L. Chen, T.-H. Kuo, H.-H. Chung, P. Huang, L.-E. Lin, C.-C. Hsu, *J. Am. Soc. Mass Spectrom.* **2021**, *32*, 653–660.
- [38] O. J. Hale, H. J. Cooper, *Anal. Chem.* **2021**, *93*, 4619–4627.
- [39] O. J. Hale, J. W. Hughes, H. J. Cooper, *Int. J. Mass Spectrom.* **2021**, *468*, 116656.
- [40] L. M. Smith, P. M. Thomas, M. R. Shortreed, L. V. Schaffer, R. T. Fellers, R. D. LeDuc, T. Tucholski, Y. Ge, J. N. Agar, L. C. Anderson, J. Chamot-Rooke, J. Gault, J. A. Loo, L. Paša-Tolić, C. V. Robinson, H. Schlüter, Y. O. Tsybin, M. Vilaseca, J. Antonio Vizcaino, P. O. Danis, N. L. Kelleher, *Nat. Methods* **2019**, *16*, 939–940.
- [41] R. E. Gossett, A. A. Frolov, J. B. Roths, W. David Behnke, A. B. Kier, F. Schroeder, *Lipids* **1996**, *31*, 895–918.
- [42] P. Carpintero, R. Anadón, S. Díaz-Regueira, J. Gómez-Márquez, *Neuroscience* **1999**, *90*, 1433–1444.
- [43] G. H. Zhang, K. D. Murthy, R. Binti Pare, Y. H. Qian, *Eur. J. Inflammation* **2020**, *18*, 2058739220934559.
- [44] D. A. Plymire, C. E. Wing, D. E. Robinson, S. M. Patrie, *Anal. Chem.* **2017**, *89*, 12030–12038.
- [45] J. M. Boggs, *Cell. Mol. Life Sci.* **2006**, *63*, 1945–1961.
- [46] P. A. C. Cloos, S. Christgau, *Biogerontology* **2004**, *5*, 139–158.
- [47] E. R. Stadtman, H. Van Remmen, A. Richardson, N. B. Wehr, R. L. Levine, *Biochim. Biophys. Acta Proteins Proteomics* **2005**, *1703*, 135–140.
- [48] T. M. Allison, P. Barran, J. L. P. Benesch, S. Cianferani, M. T. Degiacomi, V. Gabelica, R. Grandori, E. G. Marklund, T. Menneteau, L. G. Migas, A. Politis, M. Sharon, F. Sobott, K. Thalassinou, *Anal. Chem.* **2020**, *92*, 10881–10890.
- [49] S. P. Cleary, H. Li, D. Bagal, J. A. Loo, I. D. G. Campuzano, J. S. Prell, *J. Am. Soc. Mass Spectrom.* **2018**, *29*, 2067–2080.
- [50] M. T. Marty, A. J. Baldwin, E. G. Marklund, G. K. A. Hochberg, J. L. P. Benesch, C. V. Robinson, *Anal. Chem.* **2015**, *87*, 4370–4376.
- [51] D. Unsihuay, R. Yin, D. Mesa, M. Yang, Y. Li, X. Sun, S. K. Dey, J. Laskin, *Anal. Chim. Acta* **2021**, *1186*, 339085.
- [52] J. O. Kafader, R. D. Melani, K. R. Durbin, B. Ikwuagwu, B. P. Early, R. T. Fellers, S. C. Beu, V. Zabrouskov, A. A. Makarov, J. T. Maze, D. L. Shinholt, P. F. Yip, D. Tullman-Ercek, M. W. Senko, P. D. Compton, N. L. Kelleher, *Nat. Methods* **2020**, *17*, 391–394.
- [53] J. O. Kafader, K. R. Durbin, R. D. Melani, B. J. Des Soye, L. F. Schachner, M. W. Senko, P. D. Compton, N. L. Kelleher, *J. Proteome Res.* **2020**, *19*, 1346–1350.
- [54] M. A. Zenaidee, C. Lantz, T. Perkins, W. Jung, R. R. O. Loo, J. A. Loo, *J. Am. Soc. Mass Spectrom.* **2020**, *31*, 1896–1902.
- [55] L. C. Anderson, C. J. Dehart, N. K. Kaiser, R. T. Fellers, D. F. Smith, J. B. Greer, R. D. Leduc, G. T. Blakney, P. M. Thomas, N. L. Kelleher, C. L. Hendrickson, *J. Proteome Res.* **2017**, *16*, 1087–1096.
- [56] N. M. Riley, J. W. Sikora, H. S. Seckler, J. B. Greer, R. T. Fellers, R. D. Leduc, M. S. Westphall, P. M. Thomas, N. L. Kelleher, J. J. Coon, *Anal. Chem.* **2018**, *90*, 8553–8560.

Manuscript received: January 17, 2022

Accepted manuscript online: April 21, 2022

Version of record online: May 17, 2022